

Influence of the coupled-dipoles on photosynthetic performance in a photosynthetic quantum heat engine

Ling-Fang Li and Shun-Cai Zhao*

Department of Physics, Faculty of Science,

Kunming University of Science and Technology, Kunming, 650500, PR China

(Dated: January 14, 2025)

Abstract

Recent evidences suggest that the multi charge-separation pathways can contribute to the photosynthetic performance. In this work, the influence of coupled-dipoles on the photosynthetic performance was investigated in a two-charge separation pathways quantum heat engine (QHE) model. And the population dynamics of the two coupled sites, j -V characteristics and power involving this photosynthetic QHE model were evaluated for the photosynthetic performance. The results illustrate that the photosynthetic performance can be greatly enhanced but quantum interference was deactivated by the coupled-dipoles between the two-charge separation pathways. However, the photosynthetic performance can also be promoted by the deactivated quantum interference owing to the coupled-dipoles. It is a novel role of the coupled-dipoles in the energy transport process of biological photosynthetic and some artificial strategies may be motivated by this photosynthetic QHE model in future.

PACS numbers: 42.50.Gy, 42.50.-p, 32.80.Qk

Keywords: photosynthetic performance; coupled-dipole; photosynthetic heat engine

* Corresponding author: zhaosc@kmust.edu.cn.

I. INTRODUCTION

Charge separation is an essential processes in the conversion of solar energy into chemical energy in photosynthesis[1]. After absorption of a photon which creates an electronically excited state in a pigment molecule, the excited state is transformed into a short-lived charge-separated state until it arrives at a reaction center (RC)[2–6] in the pigment-protein complex and results in a stable charge-separated state, which ultimately powers the photosynthetic organism[7]. The photon-to-charge conversion efficiency in above process is considered to be close to 100% under certain conditions[8–11]. This eye-catching result sparks the researchers to explore its physics behind the energy conversion within photosynthesis[12, 13]. People firmly believe that understanding its underlying mechanism involving photosynthesis can help us in designing novel artificial nano-devices for efficient quantum transport and some optimized solar cells[14–18]. Recently, some theoretical models[19–21] show that the quantum mechanism behavior contributes beneficially to the high efficiency of biological process.

Simulating the photosynthetic RC as a biological QHE, Dorfman et al.[22] suggested that photocurrent can be improved by noise-induced coherence in the photosynthetic RC. Creatore et al.[23] have proposed a model for photosynthetic RC in which quantum mechanical effects were investigated. The results show that photo-to-charge conversion can be boosted via quantum interference caused by dipole-dipole interactions[24] between molecular excited states. And compared with classical photocell, this effect can increase the current and power output to 35%. In a multiple charge-separation pathways scheme[25], the results demonstrated that a multi-pathway biological QHE was a better choice to the charge separation then help to improve the quantum current and power yield. Recently, long-lived quantum coherence in the pigment-protein complexes was observed and extensively investigated in some experiments[1, 26–29].

Although electron transfer in the photosynthetic RC has been thoroughly investigated in one or several charge-separation pathways, and it is believed that two main pathways make significant contribution to the current and power in photosynthetic process[30]. However, works on the influence of the coupled-dipoles between two different charge separation pathways are rarely found. Therefore, we consider the coupled-dipoles between two different charge separation pathways involving the photosynthetic performance in a double-pathway[31] photosynthetic QHE model, which is different from the work discussed the system-bath couplings effect on the exciton-transfer processes in the Photosystem II reaction center via the polaron master-equation approach[32] in a QHE model. We no longer care about the impact of multi-charge-separation pathways[30, 33], but turn our attention to the impact of the coupled-dipoles on the photosynthetic performance. Focusing on this issue whether the coupled-dipoles is more beneficial to enhance the photosynthetic performances in this two-pathways biological QHE model, which can be use to mimic the process in the RC of the light-harvesting complex Phycocyanin-645 (PC645) with a pair of strongly

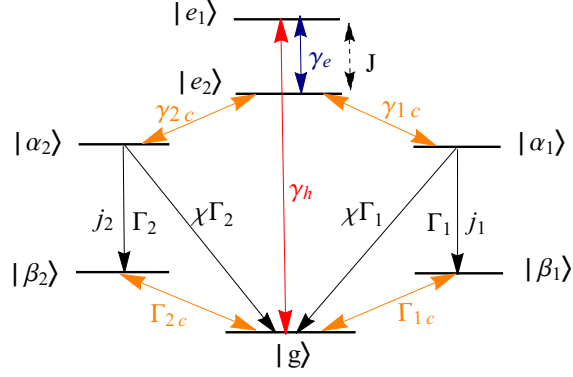


FIG. 1. (Color online) Energy-level framework of photosynthetic QHE for the photosynthetic RC with two load-transitions $|\alpha_i\rangle \rightarrow |\beta_i\rangle_{i=1,2}$. The electronic transition from the ground state $|g\rangle$ to two coupled dipoles $|e_1\rangle, |e_2\rangle$ is induced by the high temperature photon bath. The low temperature phonon bath drives charge transfer from the level $|e_2\rangle \rightarrow |\alpha_i\rangle_{i=1,2}$, and $|\beta_i\rangle_{i=1,2} \rightarrow |g\rangle$ with termination of the electronic circulation.

coupled sites (called DBV C and DBV D) [12, 34].

II. MODEL AND EQUATION

Here, we investigate the influence of the coupled-dipoles in a two-pathway QHE model illustrated in Fig.1, which is abstracted from the Photosystem II reaction center (PSII-RC) consisting of six core pigment molecules. The typical PSII-RC found in purple bacteria and in oxygen-evolving organisms (cyanobacteria, algae, and higher plants) contains six pigment molecules coupled by the dipole-dipole interactions[35–37], and the six pigments are arranged in two symmetric branches of protein matrix in the center of the complex. Four chlorophylls of them (special pair PD_1, PD_2 and accessory $ChlD_1, ChlD_2$) and two pheophytins ($PheD_1, PheD_2$), are parallel distributed in these two branches of protein matrix. The pair of chlorophylls, PD_1, PD_2 located at the center of the PSII RC act as the primary electron donors, forming two exciton states denoted as $|e_{1,2}\rangle$ in Fig.1. Two pheophytin pigments, $PheD_1$ and $PheD_2$ couple to the rest of the molecules and $PheD_1$ plays the part of electron acceptor[35–37] in the charge-separation process of the PSII RC.

As shown in Fig.1, after the absorption of a solar photon, the excited electron is promoted from $|g\rangle$ to $|e_2\rangle$ and/or $|e_1\rangle$ with the transition rate γ_h , and the excited electron may transit to $|e_1\rangle$ state at the rate γ_e . Then the excited electron is transferred to the acceptors by emission of a phonon via the two pathways: $|e_1\rangle(|e_2\rangle) \rightarrow |\alpha_1\rangle$ and $|e_1\rangle(|e_2\rangle) \rightarrow |\alpha_2\rangle$ at the emissions rates $\gamma_{ic(i=1,2)}$ with $|\alpha_1\rangle$ and $|\alpha_2\rangle$ being the ion-pair states in these two pathways. Furthermore, the positive and negative charges are spatially separated by releasing the excited electron to the plastoquinone molecule and leaving a hole in the dimer. Eventually the electron is transferred to the final electron acceptor $PheD_1$ from which the electron is

released to perform work[23] with a rate $|\Gamma_i\rangle_{(i=1,2)}$, denoted by $|\alpha_1\rangle \rightarrow |\beta_1\rangle$ (Path 1) and $|\alpha_2\rangle \rightarrow |\beta_2\rangle$ (Path 2) in Fig.1. Finally, the electron returns to the primary electron donor via $|\beta_1\rangle(|\beta_2\rangle) \rightarrow |g\rangle$. Similarly, the acceptor-to-donor charge recombination for two pathways, described by $|\alpha_1\rangle(|\alpha_2\rangle) \rightarrow |g\rangle$ with rate $\chi\Gamma_{i=1,2}$, brings the system back to the ground state $|g\rangle$ but does not produce current, where χ is a dimensionless fraction[38] describing the radiative recombination rate of the two pathways. For the physical prospective, we assume the load transition is unidirectional, which means that only the photosynthetic heat engine can transfer energy to the load, no other ways around. Therefore, the total current is given by $j = e \sum_{i=1}^2 \Gamma_i \rho_{\alpha_i \alpha_i}$ with e being the elementary electron charge.

For the purpose of clarifying the influence caused by the coupled-dipoles, we will evaluate the photosynthetic performances via the current and power involving this photosynthetic QHE numerically. Therefore, we considered the dipole-dipole coupling depicted by two excited states $|e_{1/2}\rangle = \frac{1}{\sqrt{2}}(|D_1\rangle \pm |D_2\rangle)$ [39] between the two different charge separation pathways with their eigen-energies $E_{e1/e2} = E_{D1/D2} \pm J$, where J depicts the coupling robustness illustrated in Fig.1. The state $|D_{i=1,2}\rangle$ describes chlorophylls PD_i , the electron donors. With this knowledge, the Hamiltonian of this QHE model is consisted of three parts: the electronic Hamiltonian is read as,

$$\hat{H}_e = E_g |g\rangle\langle g| + \sum_{i=1}^2 (E_{\alpha_i} |\alpha_i\rangle\langle \alpha_i| + E_{\beta_i} |\beta_i\rangle\langle \beta_i| + E_{D_i} |D_i\rangle\langle D_i|) + J(|D_1\rangle\langle D_2| + |D_2\rangle\langle D_1|), \quad (1)$$

A full microscopic mode Hamiltonian is given as follows,

$$\hat{H}_0 = \sum_k \hbar\omega_k \hat{a}_k^\dagger \hat{a}_k, \quad (2)$$

Considering above modes and ambient reservoirs linearly coupled to the electrical system[38, 40], the interaction Hamiltonian can be written in rotating-wave approximation as follows,

$$\hat{H}_v = \hat{V}_H + \hat{V}_{1c} + \hat{V}_{2c} + \hat{V}_{3c}, \quad (3)$$

where the items in above expression are given in the following forms,

$$\begin{aligned}
\hat{V}_H &= \sum_k \hbar(\varepsilon_{hk} \hat{\sigma}_{g1} \otimes \hat{a}_{hk}^\dagger + \varepsilon_{hk}^* \hat{\sigma}_{g1}^\dagger \otimes \hat{a}_{hk}), \\
\hat{V}_{1c} &= \sum_{i=1}^2 \sum_k \hbar(\varepsilon_{1ck} \hat{\sigma}_{i2} \otimes \hat{a}_{1ck}^\dagger + \varepsilon_{1ck}^* \hat{\sigma}_{i2}^\dagger \otimes \hat{a}_{1ck}), \\
\hat{V}_{2c} &= \sum_{i=1}^2 \sum_k \hbar(\varepsilon_{2ck} \hat{\sigma}_{gi} \otimes \hat{a}_{2ck}^\dagger + \varepsilon_{2ck}^* \hat{\sigma}_{gi}^\dagger \otimes \hat{a}_{2ck}), \\
\hat{V}_{3c} &= \sum_k \hbar(\varepsilon_{3ck} \hat{\sigma}_{21} \otimes \hat{a}_{3ck}^\dagger + \varepsilon_{3ck}^* \hat{\sigma}_{21}^\dagger \otimes \hat{a}_{3ck}),
\end{aligned} \tag{4}$$

where ε_{ik} ($i = h, 1c, 2c, 3c$) is the corresponding couple strength of pigment i to the k th mode of reservoir, \hat{a}_{ik}^\dagger (\hat{a}_{ik}) ($i = h, 1c, 2c, 3c$) are the creation(annihilation) operator of k th reservoir mode, the system operators are defined as $\hat{\sigma}_{g1} = |g\rangle\langle e_1|$, $\hat{\sigma}_{i2} = |\alpha_i\rangle\langle e_2|$ ($i = 1, 2$), $\hat{\sigma}_{gi} = |g\rangle\langle \beta_i|$ ($i=1,2$), and $\hat{\sigma}_{21} = |e_2\rangle\langle e_1|$.

The total system Hamiltonian, $\hat{H}_T = \hat{H}_e + \hat{H}_0 + \hat{H}_v$, where the electronic Hamiltonian \hat{H}_e describes the unitary evolution of the electron transfer via the Lindblad-type master equation,

$$\frac{d\hat{\rho}}{dt} = -i[\hat{H}_e, \hat{\rho}] + \mathcal{L}_H \hat{\rho} + \mathcal{L}_{1c} \hat{\rho} + \mathcal{L}_{2c} \hat{\rho} + \mathcal{L}_{3c} \hat{\rho} + \mathcal{L}_\Gamma \hat{\rho} + \mathcal{L}_{\chi\Gamma} \hat{\rho}, \tag{5}$$

The Lindblad-type superoperators in Eq.(5) are listed below,

$$\begin{aligned}
\mathcal{L}_H \hat{\rho} &= \frac{\gamma_h}{2} [(n_h + 1)(2\hat{\sigma}_{g1} \hat{\rho} \hat{\sigma}_{g1}^\dagger - \hat{\sigma}_{g1}^\dagger \hat{\sigma}_{g1} \hat{\rho} - \hat{\rho} \hat{\sigma}_{g1}^\dagger \hat{\sigma}_{g1}) \\
&\quad + n_h(2\hat{\sigma}_{g1}^\dagger \hat{\rho} \hat{\sigma}_{g1} - \hat{\sigma}_{g1} \hat{\sigma}_{g1}^\dagger \hat{\rho} - \hat{\rho} \hat{\sigma}_{g1} \hat{\sigma}_{g1}^\dagger)],
\end{aligned} \tag{6}$$

$$\begin{aligned}
\mathcal{L}_{1c} \hat{\rho} &= \sum_{i,j=1}^2 \frac{\gamma_{ijc}}{2} [(n_{1c} + 1)(\hat{\sigma}_{j2} \hat{\rho} \hat{\sigma}_{i2}^\dagger + \hat{\sigma}_{i2} \hat{\rho} \hat{\sigma}_{j2}^\dagger - \hat{\sigma}_{j2}^\dagger \hat{\sigma}_{i2} \hat{\rho} - \hat{\rho} \hat{\sigma}_{i2}^\dagger \hat{\sigma}_{j2}) \\
&\quad + n_{1c}(\hat{\sigma}_{i2}^\dagger \hat{\rho} \hat{\sigma}_{j2} + \hat{\sigma}_{j2}^\dagger \hat{\rho} \hat{\sigma}_{i2} - \hat{\sigma}_{i2} \hat{\sigma}_{j2}^\dagger \hat{\rho} - \hat{\rho} \hat{\sigma}_{j2} \hat{\sigma}_{i2}^\dagger)],
\end{aligned} \tag{7}$$

$$\begin{aligned}
\mathcal{L}_{2c} \hat{\rho} &= \sum_{i,j=1}^2 \frac{\Gamma_{ijc}}{2} [(n_{2c} + 1)(\hat{\sigma}_{gj} \hat{\rho} \hat{\sigma}_{gi}^\dagger + \hat{\sigma}_{gi} \hat{\rho} \hat{\sigma}_{gj}^\dagger - \hat{\sigma}_{gj}^\dagger \hat{\sigma}_{gi} \hat{\rho} - \hat{\rho} \hat{\sigma}_{gi}^\dagger \hat{\sigma}_{gj}) \\
&\quad + n_{2c}(\hat{\sigma}_{gi}^\dagger \hat{\rho} \hat{\sigma}_{gj} + \hat{\sigma}_{gj}^\dagger \hat{\rho} \hat{\sigma}_{gi} - \hat{\sigma}_{gi} \hat{\sigma}_{gj}^\dagger \hat{\rho} - \hat{\rho} \hat{\sigma}_{gj} \hat{\sigma}_{gi}^\dagger)],
\end{aligned} \tag{8}$$

$$\begin{aligned}
\mathcal{L}_{3c} \hat{\rho} &= \frac{\gamma_e}{2} [(n_e + 1)(2\hat{\sigma}_{21} \hat{\rho} \hat{\sigma}_{21}^\dagger - \hat{\sigma}_{21}^\dagger \hat{\sigma}_{21} \hat{\rho} - \hat{\rho} \hat{\sigma}_{21}^\dagger \hat{\sigma}_{21}) \\
&\quad + n_e(2\hat{\sigma}_{21}^\dagger \hat{\rho} \hat{\sigma}_{21} - \hat{\sigma}_{21} \hat{\sigma}_{21}^\dagger \hat{\rho} - \hat{\rho} \hat{\sigma}_{21} \hat{\sigma}_{21}^\dagger)],
\end{aligned} \tag{9}$$

$$\mathcal{L}_\Gamma \hat{\rho} = \sum_{i=1}^2 \frac{\Gamma_i}{2} (2\hat{\sigma}_{\alpha ii} \hat{\rho} \hat{\sigma}_{\alpha ii}^\dagger - \hat{\rho} \hat{\sigma}_{\alpha ii} - \hat{\sigma}_{\alpha ii} \hat{\rho}), \tag{10}$$

$$\mathcal{L}_{\chi\Gamma} \hat{\rho} = \sum_{i=1}^2 \frac{\chi\Gamma_i}{2} (2\hat{\sigma}_{bi} \hat{\rho} \hat{\sigma}_{bi}^\dagger - \hat{\rho} \hat{\sigma}_{\alpha ii} - \hat{\sigma}_{\alpha ii} \hat{\rho}) \tag{11}$$

Eq.(6) describes the effect of the high temperature reservoirs, where n_h denotes the average photon numbers of the high temperature reservoir, while the low temperature reservoir has the average phonon numbers $n_{1c} = [\exp(\frac{E_{e_2} - E_{\alpha_i}}{k_B T_a})]^{-1}$ in Eq.(7), $\gamma_{iic} = \gamma_{ic} (\gamma_{jjc} = \gamma_{jc})$ are the spontaneous decay rates from level $|e_2\rangle$ to level $|\alpha_i\rangle (i = 1, 2)$ respectively. The cross-coupling γ_{ijc} describes the effect of Fano interference. It is assumed that $\gamma_{ijc} = \gamma_{jic}$ with $\gamma_{ijc} = \eta_1 \sqrt{\gamma_{ic} \gamma_{jc}}$ ($i, j=1, 2$), where η_1 describes the quantum interference intensity with $\eta_1 = 1$ meaning the fully quantum interference and $\eta_1 = 0$ for no interference. Similarly, another low temperature reservoir is described by Eq.(8) with $n_{2c} = [\exp(\frac{E_{\beta_i} - E_g}{k_B T_a})]^{-1}$ being the cold reservoir phonon numbers. $\Gamma_{ijc} = \Gamma_{jic}$ is defined by $\Gamma_{ijc} = \eta_2 \sqrt{\Gamma_{ic} \Gamma_{jc}}$ in Eq.(8), which describes the Fano interference induced by the spontaneous decay rates, $\Gamma_{iic} = \Gamma_{ic} (\Gamma_{jjc} = \Gamma_{jc}) (i, j=1, 2)$ from level $|\beta_{i,(i=1,2)}\rangle$ to level $|g\rangle$ with η_2 denoting the quantum interference robustness. In Eq.(9), $n_e = [\exp(\frac{E_{e_1} - E_{e_2}}{k_B T_a})]^{-1}$ is the corresponding thermal occupation numbers of photon functioned by the robust coupled-dipoles J at temperature T_a . $\hat{\sigma}_{\alpha_{ii}} = |\alpha_i\rangle \langle \alpha_i|_{(i=1,2)}$ is defined in Eq.(10) and Eq.(11). Next, we will quantitatively depicted the electron transfer mechanisms in the photosynthetic RC via the density matrix dynamic element equations (seen in the Appendix).

III. RESULTS AND DISCUSSION

In this present model, we will explore the effect of the coupled-dipoles on the photosynthetic performance evaluated by the population dynamics of the two coupled sites, j-V characteristic and output power. For the sake of calculation, the output currents through two charge-separation pathways, $|\alpha_1\rangle \rightarrow |\beta_1\rangle$ (Path 1) and $|\alpha_2\rangle \rightarrow |\beta_2\rangle$ (Path 2) are set to be the same in the following discussion, i.e., the rates of release $\Gamma_1 = \Gamma_2$. Not only that, the total delivered voltage of the two channels is defined as the sum of their chemical potential differences between state $|\alpha_1\rangle (|\alpha_2\rangle)$ and state $|\beta_1\rangle (|\beta_2\rangle)$, $eV = \sum_{i=1}^2 [E_{\alpha_i} - E_{\beta_i} + k_B T_a \ln(\frac{\rho_{\alpha_i \alpha_i}}{\rho_{\beta_i \beta_i}})]$. The selected parameters (Shown in Table 1) E_{α_i} and E_{β_i} ($i = 1, 2$) through the two charge-separation pathways are referred to Ref.[23] with e being the elementary electron charge. Therefore, the performance of photosynthetic QHE in RC can be numerically evaluated by the current-voltage ($j - V$) characteristics and the generated power $P = j \cdot V$. Direct impact of the coupled-dipoles on the photosynthetic performance will be described by the population dynamics of the two coupled sites $|e_1\rangle$ and $|e_2\rangle$.

In Fig.2, the population dynamics of states $|e_1\rangle$ and $|e_2\rangle$ are plotted in (a1) and its inset, and the numerical output power, steady-state j-V characteristic versus different robustness of the the coupled-dipoles are illustrated in (a2) and its inset with $J=0.001, 0.005, 0.009, 0.013, 0.017$ and 0.021 . The quantum interference intensities are set as $\eta_1 = 0.35$, and $\eta_2 = 0.35$ in our numeral simulation. The antipodal influences on the two coupled sites $|e_1\rangle$ and $|e_2\rangle$ are shown by the peak populations about in the range of $[0, 100\text{fs}]$ in Fig.2 (a1). As for the excited state $|e_1\rangle$, the increasing population is generated by the more robust coupled-dipoles

TABLE I. Model parameters used in the numerical calculations.

	Values	Units
$E_{D_1} - E_g = E_{D_2} - E_g$	1.8	eV
$E_{D_1} - E_{\alpha_1} = E_{D_1} - E_{\alpha_2}$	0.2	eV
$E_{\beta_1} - E_g = E_{\beta_2} - E_g$	0.2	eV
γ_h	2.48×10^{-6}	eV
γ_e	0.025	eV
$\gamma_{1c} = \gamma_{2c}$	0.012	eV
$\Gamma_1 = \Gamma_2$	0.124	eV
$\Gamma_{1c} = \Gamma_{2c}$	0.0248	eV
n_h	6000	
T_a	300	
χ	0.2	

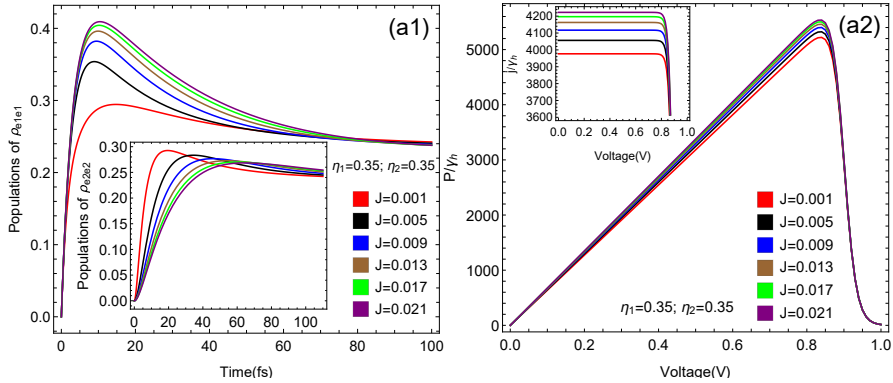


FIG. 2. (Color online) (a1) Population dynamics of level $|e_1\rangle$ and level $|e_2\rangle$, (a2) j-V characteristic and power P of this QHE with different $J = 0.001, 0.005, 0.009, 0.013, 0.017$ and 0.021 . The quantum interference intensities are selected as $\eta_1 = 0.35$ and $\eta_2 = 0.35$. Other parameters are taken from Table I.

J. However, the peak populations of $\rho_{e_2e_2}$ decrease with the increments of coupled-dipole interactions J in the same time range, $[0, 100\text{fs}]$ in Fig.2 (a1). What's more, it notes that the influence J on the peak populations in the excited state $|e_1\rangle$ is sensitive, which can be drawn from the peak differences between the purple and red curves with $J=0.001$ and 0.021 , respectively. The results indicate that more excited electrons are transferred to the exciton state $|e_1\rangle$ by the enhanced coupled-dipoles J. The large population differences indicate the better photosynthetic performance, which will be manifested by the j-V characteristic curves and output power in Fig.2 (a2). From the inset in Fig.2 (a2), the curves show that the increasing short-circuit currents and peak powers are achieved by the increments of J. The

above results demonstrate the coupled-dipoles between the two different charge separation pathways throw a positive impact on its photosynthetic performance.

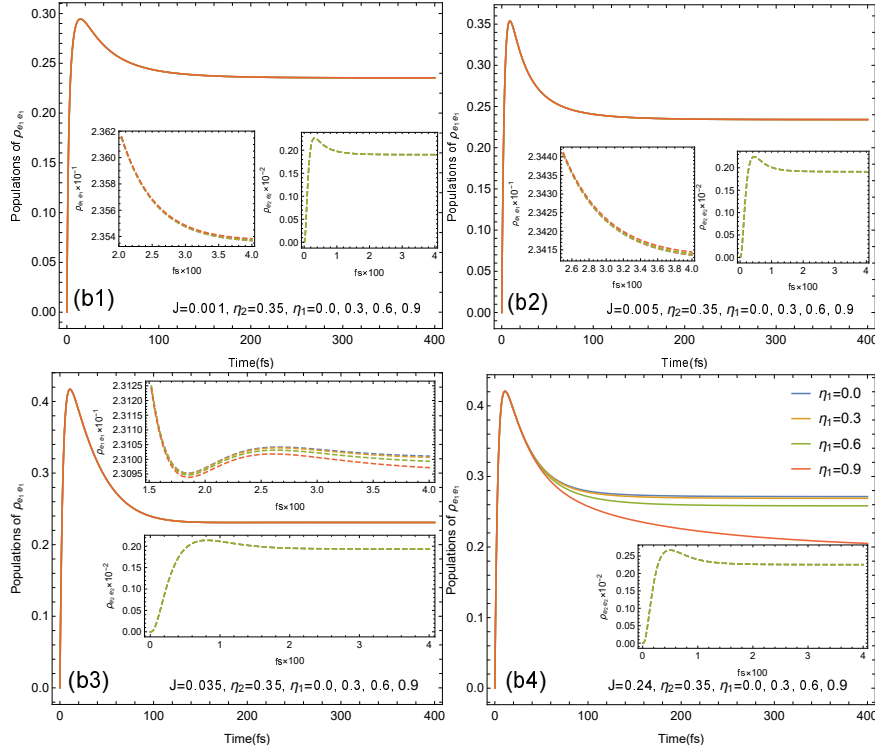


FIG. 3. (Color online) Population dynamics of level $|e_1\rangle$ and level $|e_2\rangle$ under different quantum interference intensities $\eta_1 = 0, 0.3, 0.6, 0.9$, and $\eta_2 = 0.35$ with different coupled-dipoles robustness $J=0.001, 0.005, 0.035$ and 0.24 in (b1), (b2), (b3) and (b4) respectively. Other parameters are the same to those in Fig.2.

In this proposed photosynthetic QHE model, what is the role of the coupled-dipoles between the two charge separation pathways in the Fano interference? Fig.3 demonstrates that the Fano interference caused by the cross-coupling γ_{ijc} is deactivated owing to the coupled-dipoles. In Fig.3, the population dynamics of states $|e_1\rangle$ and $|e_2\rangle$ are regulated by the Fano interference strength η_1 . Counter-intuitively, we notice that the increasing Fano interference η_1 throws almost no influence on the population dynamics of state $|e_2\rangle$, and the zoomed insets of populated $|e_1\rangle$ show minimal influence when the coupled-dipoles J is in the range of $0.001 \leq J \leq 0.035$ (cf. Fig.3 from (b1) to (b3)), as is a similar result mentioned by the previous work[25]. When the coupled-dipoles J is in the range of $0.035 \leq J \leq 0.24$, and now η_1 plays a bigger role after 60 fs (cf. the solid lines with different $\eta_1 = 0, 0.3, 0.6, 0.9$), although its impact on their peaks of population of level $|e_1\rangle$ isn't significant.

Some previous work [41] mentioned that certain “dark” states can be generated by the dipole-dipole interactions in a photosynthetic process. Maybe we can take some cues for the physical phenomenon in this proposed model, and we speculate that the coupled-dipoles between the two charge separation pathways may also produces a dark state, which disables

one chlorophylls located at the center of the PSII RC, forming one exciton state $|e_1\rangle$ being the primary electron donor. Thus, the Fano interference caused by the cross-coupling γ_{ijc} is deactivated. Changing the parameter η_1 has no substantial influence on the population dynamics of state $|e_2\rangle$. But more electrons are transferred to the exciton state $|e_1\rangle$, which ultimately results in the increasing peak population on the exciton state $|e_1\rangle$.

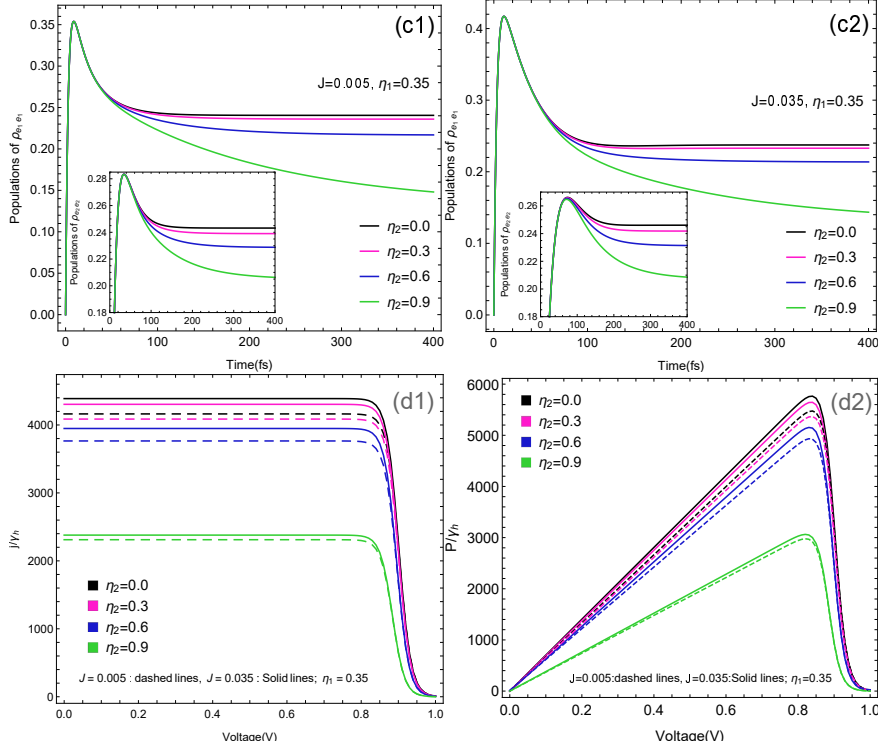


FIG. 4. (Color online) Population dynamics of level $|e_1\rangle$ and level $|e_2\rangle$ in (c1) and (c2), and j-V characteristic and power P in (d1) and (d2) with different quantum interference intensities $\eta_2 = 0, 0.3, 0.6, 0.9$, and $\eta_1 = 0.35$ under different robustness of the coupled-dipoles $J=0.005$ and $J=0.035$. Other parameters are the same to those in Fig.2

In this photosynthetic QHE system, the influence of J on another quantum interference originating from the crossing spontaneous decay rates, Γ_{1c} and Γ_{2c} from level $|\beta_{i,(i=1,2)}\rangle$ to level $|g\rangle$ stimulates our curiosity. Therefore, we similarly focus on the influence involving the robustness of J on the quantum interference described by η_2 . It notes that the inactive short-lived quantum interference η_2 still appears about in the range of $[0, 100\text{fs}]$. With the time evolution, the influence of η_2 gradually works on the population dynamics of levels $|e_1\rangle$ and $|e_2\rangle$ in the subsequent time range shown in Fig.4 (c1) and (c2). We also notice that the increasing robustness of J brings about an increment in the population difference between $|e_1\rangle$ and $|e_2\rangle$, which will indicate an enhancement of photosynthetic performance in this QHE model. The j-V characteristic and power P in (d1) and (d2) demonstrate this prediction. Curves in Fig.4 (d1) and (d2) with the same color signify the identical quantum interference η_2 . It notes that the j-V characteristic and power P increase with the

coupled-dipoles robustness J but decrease with η_2 . And the change from the dashed to solid lines with the same color manifests the enhanced photosynthetic performance due to the increasing coupled-dipoles robustness J . In this photosynthetic QHE system, the increasing η_2 indicates more electrons transiting to the state $|g\rangle$, which results in the decreasing j-V characteristic and power P in Fig.4 (d1) and (d2). The curves with the same color illustrate that the negative function of quantum interference η_2 can be suppressed by the coupled-dipoles robustness J . Finally we would like to point out that these conclusions are drawn from a typical photosynthetic RC model, it may have universal theoretical significance for the design of artificial photosynthetic devices.

IV. CONCLUSION

In this proposed photosynthetic QHE model, the roles of the coupled-dipoles between two-charge separation pathways were quantitatively explored in the photosynthetic performance. The results evaluated by the population dynamics, j-V characteristic and power P demonstrated that the photosynthetic performance was greatly enhanced but quantum interference was deactivated by the coupled-dipoles, i.e., the increasing J makes η_1 have minimal effect on the populated $|e_1\rangle$ but no effect on the populated $|e_2\rangle$ which brings out more electrons transferred to the exciton state $|e_1\rangle$ and ultimately results in the increasing peak population on the exciton state $|e_1\rangle$. However, the increasing J is beneficial to the enhancement of the photovoltaic performance evaluated by j-V characteristic and power P , although the increasing J makes η_2 have a negative influence. We argue that it is a new operating regime of the coupled-dipoles between two-charge separation pathways in the energy transport process in the biological photosynthetic, and some artificial strategies may be motivated by this photosynthetic QHE model.

V. ACKNOWLEDGMENTS

S. C. Zhao is grateful for funding from the National Natural Science Foundation of China (grants 62065009 and 61565008) and General Program of Yunnan Applied Basic Research Project, China (grant 2016FB009).

VI. APPENDIX

The density matrix dynamic element equations are given as follows:

$$\begin{aligned}
\dot{\rho}_{e_1 e_1} &= -\gamma_e[(n_e + 1)\rho_{e_1 e_1} - n_e \rho_{e_2 e_2}] - \gamma_h[(n_h + 1)\rho_{e_1 e_1} - n_h \rho_{gg}], \\
\dot{\rho}_{e_2 e_2} &= \gamma_e[(n_e + 1)\rho_{e_1 e_1} - n_e \rho_{e_2 e_2}] - \gamma_{1c}[(n_{1c} + 1)\rho_{e_2 e_2} - n_{c1}\rho_{\alpha_1 \alpha_1}] \\
&\quad - \gamma_{2c}[(n_{1c} + 1)\rho_{e_2 e_2} - n_{1c}\rho_{\alpha_2 \alpha_2}] + 2\gamma_{12c}n_{c1}Re[\rho_{\alpha_1 \alpha_2}], \\
\dot{\rho}_{\alpha_1 \alpha_1} &= \gamma_{1c}[(n_{1c} + 1)\rho_{e_2 e_2} - n_{1c}\rho_{\alpha_1 \alpha_1}] - \gamma_{12c}n_{1c}Re[\rho_{\alpha_1 \alpha_2}] \\
&\quad - (1 + \lambda)\Gamma_1\rho_{\alpha_1 \alpha_1}, \\
\dot{\rho}_{\alpha_2 \alpha_2} &= \gamma_{1c}[(n_{1c} + 1)\rho_{e_2 e_2} - n_{1c}\rho_{\alpha_1 \alpha_1}] - \gamma_{12c}n_{1c}Re[\rho_{\alpha_1 \alpha_2}] \\
&\quad - (1 + \lambda)\Gamma_2\rho_{\alpha_2 \alpha_2}, \\
\dot{\rho}_{\alpha_1 \alpha_2} &= -i\Delta_1\rho_{\alpha_1 \alpha_2} - \frac{1}{2}(\gamma_{1c} + \gamma_{2c})n_{1c}\rho_{\alpha_1 \alpha_2} \\
&\quad + \frac{1}{2}\gamma_{12c}[2(n_{1c} + 1)\rho_{e_2 e_2} - n_{1c}\rho_{\alpha_2 \alpha_2} - n_{1c}\rho_{\alpha_1 \alpha_1}] \\
\dot{\rho}_{\beta_1 \beta_1} &= \Gamma_1\rho_{\alpha_1 \alpha_1} - \Gamma_{1c}[(n_{2c} + 1)\rho_{\beta_1 \beta_1} - n_{2c}\rho_{gg}] - \Gamma_{12c}(n_{2c} + 1)Re[\rho_{\beta_1 \beta_2}], \\
\dot{\rho}_{\beta_2 \beta_2} &= \Gamma_2\rho_{\alpha_2 \alpha_2} - \Gamma_{2c}[(n_{2c} + 1)\rho_{\beta_2 \beta_2} - n_{2c}\rho_{gg}] - \Gamma_{12c}(n_{2c} + 1)Re[\rho_{\beta_1 \beta_2}], \\
\dot{\rho}_{\beta_1 \beta_2} &= -i\Delta_2\rho_{\beta_1 \beta_2} - \frac{1}{2}(\Gamma_{1c} + \Gamma_{2c})(n_{2c} + 1)\rho_{\beta_1 \beta_2} \\
&\quad - \frac{1}{2}\Gamma_{12c}[(n_{2c} + 1)\rho_{\beta_1 \beta_1} + (n_{2c} + 1)\rho_{\beta_2 \beta_2} - 2n_{2c}\rho_{gg}], \\
\rho_{gg} &= 1 - \rho_{e_1 e_1} - \rho_{e_2 e_2} - \rho_{\alpha_1 \alpha_1} - \rho_{\alpha_2 \alpha_2} - \rho_{\beta_1 \beta_1} - \rho_{\beta_2 \beta_2}.
\end{aligned} \tag{12}$$

where $\Delta_1 = E_{\alpha_1} - E_{\alpha_2}$ and $\Delta_2 = E_{\beta_1} - E_{\beta_2}$ are the splitting of the states $|\alpha_1\rangle(|\alpha_2\rangle)$ and $|\beta_1\rangle(|\beta_2\rangle)$. We utilize the equations to simulate dynamics of the reaction centre.

-
- [1] G. S. Engel, T. R. Calhoun, E. L. Read, T. K. Ahn, T. Mancal, Y. C. Cheng, R. E. Blankenship, and G. R. Fleming. Evidence for wavelike energy transfer through quantum coherence in photosynthetic systems. *Nature*, 446(7137):782, 2007.
 - [2] L. Akihito and G. R. Fleming. Theoretical examination of quantum coherence in a photosynthetic system at physiological temperature. *Proceedings of the National Academy of Sciences of the United States of America*, 106(41):17255, 2009.
 - [3] J. Zhu, S. Kais, P. Rebentrost, and A. Aspuru-Guzik. Modified scaled hierarchical equation of motion approach for the study of quantum coherence in photosynthetic complexes. *Journal of Physical Chemistry B*, 115(6):1531, 2011.
 - [4] J. R. Caram, N. H. C. Lewis, A. F. Fidler, and G. S. Engel. Signatures of correlated excitonic dynamics in two-dimensional spectroscopy of the fenna-matthew-olson photosynthetic complex. *Journal of Chemical Physics*, 136(10):17255, 2012.
 - [5] P. Rebentrost, M. Mohseni, I. Kassal, S. Lloyd, and A. Aspuru-Guzik. Environment-assisted quantum transport. *New Journal of Physics*, 11(3):033003, 2009.

- [6] N. Killoran, S. F. Huelga, and M. B. Plenio. Enhancing light-harvesting power with coherent vibrational interactions: A quantum heat engine picture. *Journal of Chemical Physics*, 143(15):155102, 2015.
- [7] Mohseni M, Rebentrost P, Lloyd S, and Aspuru-Guzik A. Environment-assisted quantum walks in photosynthetic energy transfer. *Journal of Chemical Physics*, 129(17):174106, 2008.
- [8] Z. Esták. Blankenship, R. E.: Molecular mechanisms of photosynthesis. *Photosynthetica*, 40(1):12, 2002.
- [9] J. Gilmore and R. H. McKenzie. Quantum dynamics of electronic excitations in biomolecular chromophores: Role of the protein environment and solvent. *Journal of Physical Chemistry A*, 112(11):2162, 2008.
- [10] F. Caruso, A. W. Chin, A. Datta, S. F. Huelga, and M. B. Plenio. Highly efficient energy excitation transfer in light-harvesting complexes: The fundamental role of noise-assisted transport. *Journal of Chemical Physics*, 131(10):105106, 2009.
- [11] H. B. Chen, P. Y. Chiu, and Y. N. Chen. Vibration-induced coherence enhancement of the performance of a biological quantum heat engine. *Phys. Rev. E*, 94(5):052101, 2016.
- [12] E. Collini, C. Y. Wong, K. E. Wilk, P. M. G. Curmi, P. Brumer, and G. D. Scholes. Coherently wired light-harvesting in photosynthetic marine algae at ambient temperature. *Nature*, 463(7281):644, 2010.
- [13] E. Romero, R. Augulis, V. I. Novoderezhkin, M. O. Ferretti, J. Thieme, D. Zigmantas, and R. V. Grondelle. Quantum coherence in photosynthesis for efficient solar-energy conversion. *Nat. Phys.*, 10(9):676, 2014.
- [14] S. C. Zhao and J. Y. Chen. Enhanced quantum yields and efficiency in a quantum dot photocell modeled by a multi-level system. *New Journal of Physics*, 21(10):103015, 2019.
- [15] B. P. Fingerhut, W. Zinth, and R. de Vivie-Riedle. The detailed balance limit of photochemical energy conversion. *Phys. Chem. Chem. Phys.*, 12:422, 2010.
- [16] J. Y. Chen and S. C. Zhao. Inhibited radiative recombination rate to enhance quantum yields in a quantum photocell. *Chinese Physics B*, 29(6), 2020.
- [17] R. E. Blankenship, D. M. Tiede, J. Barber, G. W. Brudvig, G. Fleming, M. Ghirardi, M. R. Gunner, W. Junge, D. M. Kramer, A. Melis, T. A. Moore, C. C. Moser, D. G. Nocera, D. R. Parson W. W. Nozik, A. J. Ort, R. C. Prince, and R. T. Sayre. Comparing photosynthetic and photovoltaic efficiencies and recognizing the potential for improvement. *Science*, 805:332, 2011.
- [18] S. C. Zhao, J. Y. Chen, and X. Li. Different roles of quantum interference in a quantum dot photocell with two intermediate bands. *The European Physical Journal Plus*, 135(892):1–10, 2020.
- [19] G. R. Fleming. Theoretical examination of quantum coherence in a photosynthetic system at physiological temperature. *Proceedings of the National Academy of Sciences*, 106(41):17255, 2009.

- [20] S. F. Huelga and M. B. Plenio. Vibrations, quanta and biology. *Contemporary Physics*, 54(4):181, 2013.
- [21] X. L. Zong, W. Song, J. Zhou, M. Yang, L. B. Yu, and Z. L. Cao. Enhancing the absorption and energy transfer process via quantum entanglement. *Quantum Information Processing*, 17(7):158, 2018.
- [22] K. E. Dorfman, D. V. Voronine, S. Mukamel, and M. O. Scully. Photosynthetic reaction center as a quantum heat engine. *Proceedings of the National Academy of Sciences*, 110(8):2746, 2013.
- [23] C. Creatore, M. A. Parker, S. Emmott, and A. W. Chin. An efficient biologically-inspired photocell enhanced by quantum coherence. *Phys. Rev. Lett.*, 111:253601, 2013.
- [24] S. H. Su, X. Q. Luo, J. C. Chen, and C. P. Sun. Angle-dependent quantum otto heat engine based on coherent dipole-dipole coupling. *Europhysics Letters*, 115(3):30002, 2016.
- [25] M. Qin, H. Z. Shen, and X. X. Yi. A multi-pathway model for photosynthetic reaction center. *Journal of Chemical Physics*, 144(12):125103, 2016.
- [26] G. Panitchayangkoon, D. Hayes, K. A. Fransted, J. R. Caram, E. Harel, J. Wen, R. E. Blankenship, and G. S. Engel. Long-lived quantum coherence in photosynthetic complexes at physiological temperature. *Proceedings of the National Academy of Sciences of the United States of America*, 107(29):12766, 2010.
- [27] E. Collini, C. Y. Wong, K. E. Wilk, P. M. G. Curmi, P. Brumer, and G. D. Scholes. Coherently wired light-harvesting in photosynthetic marine algae at ambient temperature. *Nature*, 463(7281):644, 2010.
- [28] P. Huo and D. F. Coker. Iterative linearized density matrix propagation for modeling coherent excitation energy transfer in photosynthetic light harvesting. *Journal of Chemical Physics*, 133(18):184108, 2010.
- [29] N. Christensson, H. F. Kauffmann, T. Pullerits, and T. Manal. Origin of long-lived coherences in light-harvesting complexes. *Journal of Physical Chemistry B*, 116(25):7449, 2012.
- [30] A. Cardona, T. Sedoud, N. Cox, and R. A. William. Charge separation in photosystem II: A comparative and evolutionary overview. *Biochimica et Biophysica Acta (BBA)- Bioenergetics*, 1817(1):26, 2012.
- [31] T. B. Arp, Y. Barlas, V. Aji, and N. M. Gabor. Natural regulation of energy flow in a green quantum photocell. *Nano Letters*, 16(12):7461, 2015.
- [32] M. Qin, H. Z. Shen, X. L. Zhao, and X. X. Yi. Effects of system-bath coupling on a photosynthetic heat engine: A polaron master-equation approach. *Physical Review A*, 96(1):012125, 2017.
- [33] X. X. Yi. A multi-pathway model for photosynthetic reaction center. *Journal of Chemical Physics*, 144(12):625, 2015.
- [34] A. P. Leonardo and B. Paul. Physical basis for long-lived electronic coherence in photosynthetic light-harvesting systems. *Journal of Physical Chemistry Letters*, 2(21):2728, 2011.
- [35] V. I. Novoderezhkin, J. P. Dekker, and R. Van Grondelle. Mixing of exciton and charge-

- transfer states in photosystem ii reaction centers: Modeling of stark spectra with modified redfield theory. *Biophysical Journal*, 93(4):1293, 2007.
- [36] R. V. Elisabet, I. H. M. Stokkum, V. I. Novoderezhkin, J. P. Dekker, and R. V. Grondelle. Two different charge separation pathways in photosystem II. *Biochemistry*, 49(20):4300, 2010.
- [37] V. I. Novoderezhkin, E. Romero, J. P. Dekker, and R. V. Grondelle. Multiple charge-separation pathways in photosystem ii: modeling of transient absorption kinetics. *Chemphyschem A European Journal of Chemical Physics and Physical Chemistry*, 12(3):681, 2015.
- [38] J. Y. Chen and S. C. Zhao. Radiative recombination rate suppressed in a quantum photocell with three electron donors. *The European Physical Journal Plus*, 135(92):1–8, 2020.
- [39] H. B. Chen, J. Y. Lien, C. C. Hwang, and Y. N. Chen. Long-lived quantum coherence and non-markovianity of photosynthetic complexes. *Physical Review E*, 89(4):42147–42147, 2014.
- [40] S. C. Zhao and Q. X. Wu. High quantum yields generated by a multi-band quantum dot photocell. *Superlattices and Microstructures*, 137:106329, 2020.
- [41] Y. T. Zhang, S. Oh, F. H. Alharbi, G. S. Engel, and S. Kais. Delocalized quantum states enhance photocell efficiency. *Physical Chemistry Chemical Physics*, 17(8):5743, 2015.

